Vascular Photoacoustic Volume Registration via 2D Feature Matching with Reverse Mapping Based on Maximum Intensity Projection

Junda Liao[1,4], Chu Zhou[4], Yuta Asano[4], Yushi Suzuki[2], Ryoma Bise[3], Nobuaki Imanishi[2], Kazuo Kishi[2], Sadakazu Aiso[2], and Imari Sato[1,4]

[1] The University of Tokyo, Tokyo, Japan
liao-junda@g.ecc.u-tokyo.ac.jp
[2] Keio University, Tokyo, Japan
[3] Kyushu University, Fukuoka, Japan
[4] National Institute of Informatics, Tokyo, Japan

Abstract. Photoacoustic (PA) imaging is an emerging biomedical imaging modality well-suited for visualizing blood vessels due to its non-invasive, label-free nature. Registering vascular PA volumetric images acquired at different times or viewpoints is crucial for tracking longitudinal changes and expanding the field of view for comprehensive vascular assessment. However, PA volumes exhibit characteristics such as sparsity, ambiguity, vascular network changes, and unavoidable body hair, which pose significant challenges and limit the accuracy and robustness of existing registration methods. We propose a robust affine registration framework to address PA registration challenges, integrating feature-based alignment, intensity-based refinement, and hair removal. We leverage 2D feature matching with reverse mapping based on maximum intensity projections (MIPs) to handle sparsity and ambiguity, enabling robust alignment. An intensity-based refinement further enhances accuracy by incorporating our feature-guided sampling strategy to mitigate the impact of vascular network changes. Additionally, we introduce a hair removal procedure to prevent hairs from affecting registration. Experimental evaluation, conducted in collaboration with medical experts, demonstrates that our method outperforms existing approaches in both accuracy and robustness on real PA volumes.

Keywords: Photoacoustic · Image Registration · Vasculature

1 Introduction

Photoacoustic imaging (PAI) is a hybrid imaging modality based on the photoacoustic effect [5]. As illustrated in Fig. 1(a), PAI uses laser pulses to irradiate tissue, where chromophores such as hemoglobin absorb the light and generate ultrasonic waves through thermoelastic expansion. These waves are then detected by ultrasound sensors and reconstructed into images. With its non-invasive, label-free nature, and high spatial resolution, PAI provides an effective way for

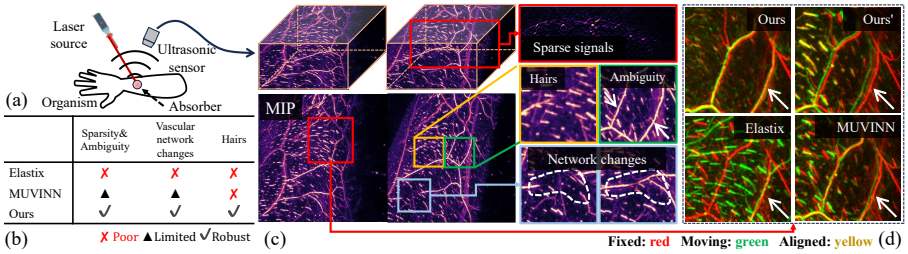

Fig. 1. (a) Principle of PAI. (b) Comparison of our method with baseline methods, MUVINN [7] and Elastix [16]. (c) Challenges in vascular PA volume registration. From top to bottom: a slice view of a PA volume (sparsity), hair artifacts, two visually similar vessels indicated by while arrows (ambiguity), and a missing vessel in one volume (vascular network changes). (d) Zoomed-in registration results.

visualizing vascular structures, which often serve as clues for disease detection. Unlike magnetic resonance imaging (MRI), PAI does not require contrast agents or extra preparation [2].

In vascular PAI, aligning volumes acquired at different times or from different viewpoints is essential for tracking longitudinal changes and expanding the field of view for a more comprehensive vascular assessment. However, the characteristics of vascular PA volumes present four key challenges for registration, as illustrated in Fig. 1(c): (1) Sparsity: unlike dense anatomical structures in MRI or computed tomography (CT) images (e.g., brain), blood vessels in PA volumes are sparse, occupying a small fraction of the volume. Efficiently handling this sparsity is crucial for robust and accurate registration. (2) Ambiguity: vessels with similar width and orientation are difficult to distinguish, introducing ambiguity in correspondence establishment. (3) Vascular network changes: factors such as acquisition settings, treatment effects, or disease progression can cause the same vessels to differ in width and intensity. Some vessels may even be missing in certain PA volumes. (4) Hair artifacts: hair produces strong signals in PA imaging and short hairs may persist even after shaving. Its deformations often differ from those of vessels, causing vessel misalignment even when hairs are correctly registered. This effect is evident in the registration results with and without hair removal using our method in Fig. 1(d).

Some studies on vascular PA volume registration focus on aligning batches of PA volumes from multi-scan acquisitions to enhance image quality [6,1,13], which differs from the goal of pairwise registration for volumes acquired at different times or viewpoints. Prior pairwise vascular PA volume registration studies [30,7] have applied intensity-based registration, a widely used approach in medical image registration [16,28,27,21,20,3,1,12], which aligns images by comparing voxel intensity distributions using similarity measures such as mutual information (MI). Yu et al. [30] compare various registration schemes and emphasize the importance of initialization for intensity-based methods. De Santi et al. [7] employ implicit neural representations (INRs) to model the displacement field and

address sparsity using a multi-resolution strategy with importance sampling. While intensity-based methods achieve high accuracy, they are prone to local minima and heavily depend on initialization when handling large misalignments. This is due to their reliance on non-smooth similarity metrics with numerous local extrema [23]. The sparsity, ambiguity, vascular network changes, and hair artifacts in vascular PA volumes further exacerbate this issue.

Feature-based methods estimate transformations by extracting and matching features [19,18,4,25], demonstrating robustness to large misalignments when sufficient keypoints are matched. Yu et al. [29] propose an unsupervised learning model for obtaining matched keypoints in brain MRI volumes, utilizing a closed-form solution for affine registration, demonstrating strong robustness. However, its application to PA volumes is hindered by limited training data. Rister et al. [24] extend SIFT [18] for volumetric image registration but show limited robustness in vascular PA volumes, likely due to the absence of distinct corner- or blob-like features. While recent learning-based feature matching methods perform well across various image domains, they are predominantly designed for 2D images. Moreover, applying 2D feature matching on slices is impractical due to sparse signals and indistinguishable appearance of vessels in slice views.

In this paper, we propose a robust affine registration framework for vascular PA volumes that integrates feature-based alignment for robustness, intensity-based refinement for accuracy, and hair removal to mitigate the impact of hair artifacts on registration. Our key contribution is a novel feature-based registration pipeline that leverages 2D feature matching with reverse mapping to handle sparsity and ambiguity by shifting the registration problem from whole-volume processing to a set of keypoints, enabling robust registration against large misalignments. Specifically, we extract and match keypoints from the maximum intensity projections (MIPs) of PA volumes along the depth axis using recent advances in learnable local feature matching, then reverse-map the keypoints to 3D positions to estimate the transformation. To achieve higher accuracy, we refine the transformation using an intensity-based approach with our proposed feature-guided sampling strategy, ensuring optimization focuses on consistent vascular structures and effectively handling vascular network changes. Additionally, we propose a clustering-based hair removal procedure that utilizes prior knowledge of hair characteristics to minimize their impact on vessel alignment.

In summary, the main contributions of this work are as follows:

1. Novel feature-based registration pipeline that integrates 2D feature matching with reverse mapping to effectively address sparsity and ambiguity.
2. Feature-guided sampling strategy that enhances robustness against vascular network changes for intensity-based refinement.
3. Hair removal procedure as a preprocessing step to mitigate hair artifacts.

2 Method

Let V_f and V_m be the fixed (target) and moving (source) volumes. We aim to find the optimal affine transformation matrix $\mathcal{A}^* \in \mathbb{R}^{4\times4}$ so that the transformed

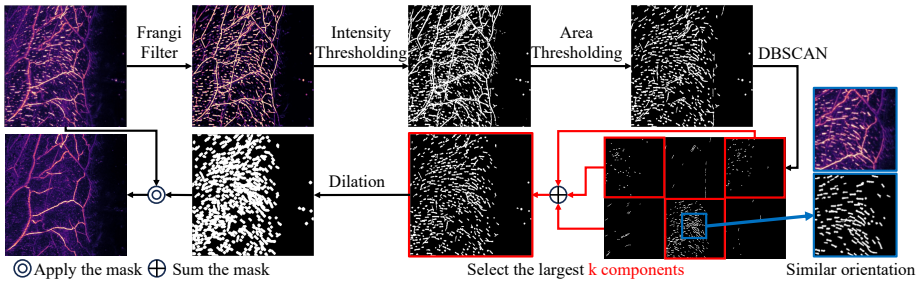

Fig. 2. Diagram of the proposed hair removal procedure. All operations are applied to volumes; MIPs are shown for illustration purposes.

volume $V_m \circ \mathcal{A}^*$ aligns with V_f. We assume both V_f and V_m are grayscale vascular PA volumes. Our framework first removes hairs if present. We then extract and match 2D keypoints from the MIPs of the PA volumes, reverse-map them to 3D positions, and estimate an initial affine transformation. Finally, intensity-based refinement with feature-guided sampling further improves alignment.

2.1 Hair Removal

To focus registration on vessels rather than hairs, we introduce a hair removal procedure. A previous study [15] employed a semi-supervised approach for hair removal in PA volumes but demonstrated limited generalizability. To eliminate the need for additional labeling, we propose a clustering-based method that leverages prior knowledge of hair characteristics.

The hair removal procedure, illustrated in Fig. 2, begins with the Frangi filter [11] to enhance tubular structures and suppress background noise. Thresholding is then applied for initial segmentation, followed by retaining only regions within a predefined size range, as hair regions are generally shorter than vessel regions. The retained regions consist primarily of hair, along with some vessels. To further differentiate hair regions from vessels, we apply DBSCAN clustering [9], leveraging the observation that adjacent body hairs often share similar orientations and distinct intensity distributions compared to vessels [15]. Clustering features include region orientation and intensity histogram. The largest k clusters ($k = 3$ in this work) are identified as hair regions and removed by zeroing or inpainting the corresponding voxels. While not perfectly accurate, the removal effectively prevents hair artifacts from interfering with registration.

2.2 Feature-based Alignment with Reverse-Mapping

To exploit recent advances in 2D learning-based feature matching for PA volume registration, we introduce a reverse mapping approach inspired by critical point detection in tree-like structures [26,17,31]. Handcrafted feature models like SIFT exhibit limited effectiveness on vascular PA volumes [30]. While learning-based methods outperform them, most are designed exclusively for 2D images.

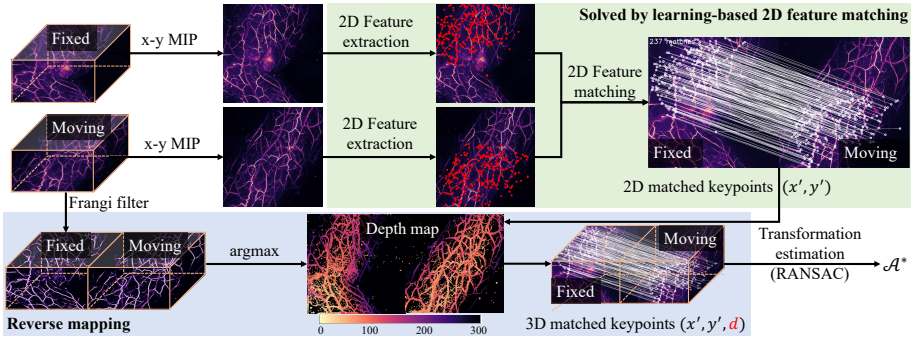

Fig. 3. Diagram of the proposed feature-based alignment with reverse mapping.

However, due to the sparsity of PA volumes, vascular structures are often well-separated in their MIPs. This enables effective 3D transformation estimation using reverse-mapped keypoints in 3D from 2D feature matching on MIPs.

Reverse mapping relies on the observation that a 2D vessel point in the x-y MIP corresponds to the 3D voxel with the same (x, y) coordinates and the maximum intensity along the depth axis. As illustrated in Fig. 3, to determine the corresponding depth d of a keypoint (x', y') on the MIP, we perform reverse mapping as $d = \arg\max_z \mathcal{F}(V, \sigma)(x', y', z)$, where $\mathcal{F}$ is the Frangi filter, which suppresses background noise to improve reverse mapping accuracy, and σ (set to 4 in this work) controls the scale of vessels enhanced. Building on this, we extract and match keypoints from the x-y MIPs of V_f and V_m, then reverse-map them back to 3D space. For this, we select OmniGlue [14] due to its strong generalizability to PA volume MIPs, despite not being explicitly trained on them. We use the publicly released model weights without any additional fine-tuning.

Given N matched keypoints $(p_i, q_i)_{i=1}^N$, where $p_i, q_i \in \mathbb{R}^3$ are keypoints detected in V_m and V_f, respectively, the optimal affine transformation $\mathcal{A}^*$ is computed by solving $\mathcal{A}^* = \arg\min_{\mathcal{A}} \sum_{i=1}^N \|q_i - \mathcal{A}\tilde{p}_i\|^2$, where $\tilde{p}_i = [p_i^\top; 1]^\top \in \mathbb{R}^4$ represents the homogeneous coordinates of p_i. This optimization problem is efficiently and robustly solved using the total least squares method with RANSAC [10].

2.3 Intensity-based Refinement with Feature-guided Sampling

Given the good initialization provided by the preceding feature-based alignment, we apply intensity-based registration with our proposed feature-guided sampling strategy to further improves registration accuracy.

To achieve this, we adopt a typical iterative optimization framework [16]. However, similarity measures become less reliable in regions with vascular network changes, increasing the risk of suboptimal registration. To overcome this, we use keypoints from feature-based alignment to guide sampling, ensuring optimization focuses on regions with consistent vascular structures. Specifically, all

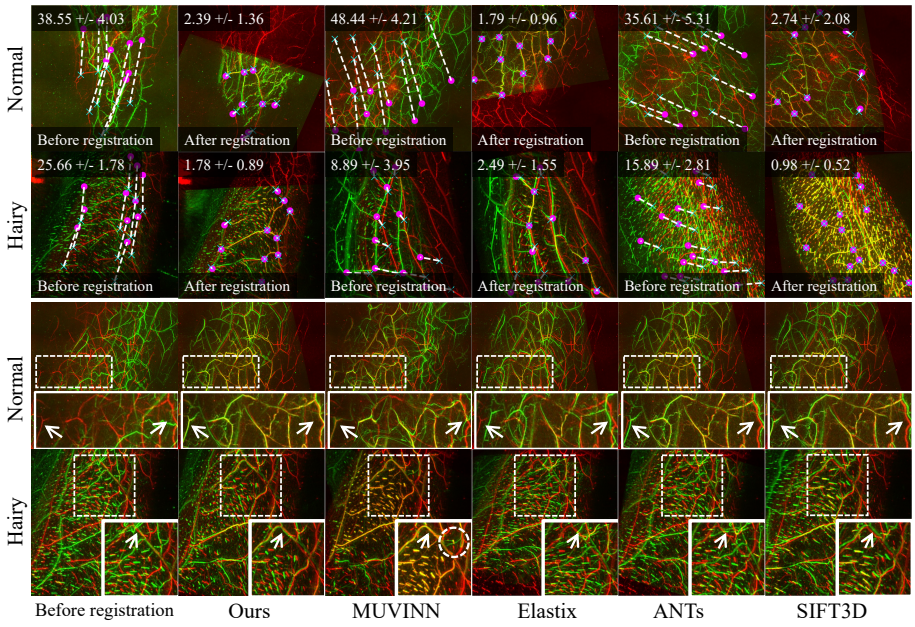

Fig. 4. Top: Registration results of our method with TRE scores (mm) in the upper left corner. Fixed landmarks: crosses, moving landmarks: circles. **Bottom**: Comparison of baseline methods and our approach. All results are shown as x-y MIPs, with hairs added back to the registration results of hairy data in our approach for fair comparison

inlier keypoints identified by RANSAC in V_f serve as centers for $n \times n \times n$ patches ($n = 5$ in this work), from which 20% of voxels are randomly sampled per iteration to compute the similarity measure. To emphasize vascular structures and suppress background noise, we perform optimization on the Frangi filter output ($\sigma = 2$) instead of the original PA volumes. MI is used as the similarity measure for its robustness to intensity variations. The optimization problem is formulated as $\mathcal{A}^* = \arg\min_{\mathcal{A}} \mathrm{MI}(\mathcal{F}(V_f, \sigma), \mathcal{F}(V_m, \sigma) \circ \mathcal{A})$, where $\circ$ denotes applying the transformation to a volume.

3 Experiments

We evaluated the proposed framework on 20 pairs of vascular PA volumes, including 10 without hairs (normal dataset) and 10 with hairs (hairy dataset), acquired from the leg and arm at different time points using a PA imaging system [22] with 797 nm incident light. Regions of interest were manually cropped, yielding volumes ranging from $800 \times 800 \times 300$ to $1200 \times 1200 \times 300$ with a voxel size of $[0.1, 0.1, 0.1]$ mm. Code available: https://codeberg.org/ljd/pa-reg.

For quantitative evaluation, we manually annotated matched landmarks for each volume pair under the guidance of a medical expert to compute the Target

Table 1. Quantitative comparisons with baselines. Standard deviations are in parentheses. All results represent average scores across the dataset. Before-reg refers to before registration. ↑ (↓) indicates that higher (lower) values are better.

Method	Normal		Hairy		Time (s)
	TRE (mm) ↓	Dice↑	TRE (mm) ↓	Dice↑	
Before-reg	27.82 (9.74)	0.02 (0.02)	15.08 (7.20)	0.06 (0.07)	-
Ours	**1.30 (0.72)**	**0.46 (0.19)**	**1.34 (0.31)**	**0.44 (0.18)**	11.27
Elastix	21.02 (14.06)	0.16 (0.19)	14.24 (9.06)	0.26 (0.22)	22.98
ANTs	13.73 (17.97)	0.22 (0.22)	14.61 (8.25)	0.21 (0.20)	659.74
MUVINN	25.53 (12.59)	0.18 (0.14)	14.39 (10.97)	0.12 (0.07)	1243.51
SIFT3D	11.32 (17.15)	0.26 (0.18)	6.51 (4.49)	0.30 (0.21)	65.64

Table 2. Quantitative results of ablation studies on hair removal (HR), feature-based alignment (FA), intensity-based refinement (IR), IR with uniform sampling (IR′), and FA using 2D SIFT (FA′).

Method	Normal		Hairy	
	TRE (mm) ↓	Dice ↑	TRE (mm) ↓	Dice ↑
Ours	**1.30 (0.72)**	**0.46 (0.19)**	**1.34 (0.31)**	**0.44 (0.18)**
w/o HR	**1.30 (0.72)**	**0.46 (0.19)**	2.28 (0.92)	0.40 (0.14)
w/o FA	23.61 (13.83)	0.15 (0.17)	15.11 (8.46)	0.19 (0.22)
w/o IR	2.21 (1.56)	0.40 (0.23)	2.42 (1.58)	0.38 (0.16)
w/ IR′	1.92 (2.58)	0.42 (0.20)	2.22 (1.03)	0.41 (0.15)
w/ FA′	14.89 (19.95)	0.28 (0.22)	24.31 (20.57)	0.14 (0.15)

Registration Error (TRE) [23], defined as the average Euclidean distance between corresponding landmarks. Additionally, we computed the Dice score [8] to quantify the spatial overlap between vessel regions in the fixed and moving PA volumes. Vessel segmentation masks were obtained via thresholding, with hair regions removed in hairy data using the proposed hair removal procedure.

We evaluated our method against two widely used classical intensity-based medical image registration frameworks, Elastix [16] and ANTs [28], as well as SIFT3D [24], a feature-based approach, and MUVINN [7], an INR-based method for PA registration that is not limited to affine registration.

3.1 Results

Table 1 shows that our method outperforms all baselines across both datasets. SIFT3D exhibits large variations, indicating limited robustness for PA volumes. ANTs performs well on some normal cases but struggles with most hairy ones. Elastix and MUVINN succeed only in a few instances. MUVINN fails due to the lack of transformation constraints, causing it to register unrelated vessels non-rigidly and converge to local minima. Our results suggest that affine transforma-

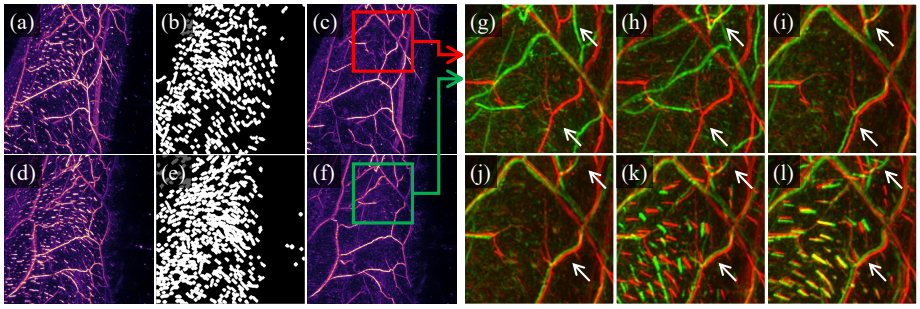

Fig. 5. (a–c) Fixed volume, its hair mask, and hair-removed fixed volume. (d–f) Moving volume, its hair mask, and hair-removed moving volume. (g) Zoomed-in regions (red and green boxes) before registration. (h) Registration without feature-based alignment. (i) Registration without intensity-based refinement. (j) Registration using the full pipeline. (k) Hairs added back to (j). (l) Registration without hair removal.

tion is sufficient to correct most misalignments, as vascular structures rarely undergo significant changes unless extensive vascular surgery has been performed.

Fig. 4 presents qualitative results, and we provide 3D visualizations in the supplementary material. In the normal example, our method successfully aligns the vessels marked by white arrows. MUVINN fails entirely, while SIFT3D, ANTs, and Elastix correct most misalignments but still leave residual errors at the white arrow-marked locations. In the hairy example, our method effectively focuses on vessels, as indicated by the misaligned hairs within the white box in Fig. 4. Elastix and ANTs fail completely, MUVINN achieves most affine alignment but introduces distortions (white circle), and SIFT3D attempt to align hairs, resulting in less accurate vessel registration than our method.

3.2 Ablation Study

We perform ablation studies to evaluate the contribution of each step in our method. Table 2 shows that removing any step degrades performance. Notably, excluding feature-based alignment leads to a significant drop, emphasizing its role in correcting large misalignments. Replacing feature-guided sampling with uniform sampling (w/ IR′) improves results over omitting intensity-based refinement (w/o IR) but remains inferior to the full pipeline, demonstrating its effectiveness. Additionally, 2D SIFT shows large performance variations, further highlighting the limitations of handcrafted features for PA data.

Fig. 5 provides a qualitative example alongside hair removal results. Fig. 5(h) shows that intensity-based registration alone fails to correct misalignment. Fig. 5(i-j) illustrate how intensity-based refinement resolves minor residual displacements, especially in vessels marked by white arrows. Meanwhile, Fig. 5(j-l) show how hairs misguides registration, causing vessel misalignment despite hairs being correctly registered, emphasizing the necessity of hair removal.

4 Conclusion

We propose a vascular PA volume registration framework that integrates feature-based alignment, intensity-based refinement, and hair removal. Our method leverages 2D feature matching with reverse mapping for robust alignment despite sparsity and ambiguity. Intensity-based refinement further improves registration accuracy, with our feature-guided sampling enhances to handle vascular network changes. Moreover, hair removal ensures registration focuses on vessels. Experimental results confirm the robustness and accuracy of our method on real vascular PA volumes. For future work, we aim to address inaccurate registration caused by feature matching failures due to significant non-rigid deformations or minimal overlap in vascular PA volumes.

Acknowledgments. This research was supported by JST-Mirai Program under Grant Number JPMJM123G1 and AMED under Grant Number JP19he2302002.

Disclosure of Interests. The authors have no competing interests to declare that are relevant to the content of this article.

References

1. Asanomi, T., Nishimura, K., Song, H., Hayashida, J., Sekiguchi, H., Yagi, T., Sato, I., Bise, R.: Unsupervised Deep Non-rigid Alignment by Low-Rank Loss and Multi-input Attention. In: Proc. of the Medical Image Computing and Computer-Assisted Intervention. vol. 13436, pp. 185–195 (2022)
2. Attia, A.B.E., Balasundaram, G., Moothanchery, M., Dinish, U., Bi, R., Ntziachristos, V., Olivo, M.: A review of clinical photoacoustic imaging: Current and future trends. Photoacoustics **16**, 100144 (2019)
3. Balakrishnan, G., Zhao, A., Sabuncu, M.R., Guttag, J., Dalca, A.V.: VoxelMorph: A Learning Framework for Deformable Medical Image Registration. IEEE Transactions on Medical Imaging **38**(8), 1788–1800 (2019)
4. Bay, H., Tuytelaars, T., Van Gool, L.: SURF: Speeded Up Robust Features. In: Computer Vision – ECCV 2006. pp. 404–417 (2006)
5. Bell, A.G.: On the production and reproduction of sound by light. American journal of science **3**(118), 305–324 (1880)
6. Bise, R., Zheng, Y., Sato, I., Toi, M.: Vascular Registration in Photoacoustic Imaging by Low-Rank Alignment via Foreground, Background and Complement Decomposition. In: Proc. of the Medical Image Computing and Computer-Assisted Intervention. vol. 9902, pp. 326–334 (2016)
7. De Santi, B., Kim, L., Bulthuis, R.F.G., Lucka, F., Manohar, S.: Automated three-dimensional image registration for longitudinal photoacoustic imaging. J. Biomed. Opt. **29**(S1) (2024)
8. Dice, L.R.: Measures of the amount of ecologic association between species. Ecology **26**(3), 297–302 (1945)
9. Ester, M., Kriegel, H.P., Sander, J., Xu, X.: A density-based algorithm for discovering clusters in large spatial databases with noise. In: Proceedings of the Second International Conference on Knowledge Discovery and Data Mining. pp. 226–231. KDD'96 (1996)

10. Fischler, M.A., Bolles, R.C.: Random sample consensus: A paradigm for model fitting with applications to image analysis and automated cartography. Commun. ACM **24**(6), 381–395 (1981)
11. Frangi, A.F., Niessen, W.J., Vincken, K.L., Viergever, M.A.: Multiscale vessel enhancement filtering. In: Proc. of the Medical Image Computing and Computer-Assisted Intervention. vol. 1496, pp. 130–137 (1998)
12. Hering, A., Van Ginneken, B., Heldmann, S.: mlVIRNET: Multilevel Variational Image Registration Network. In: Proc. of the Medical Image Computing and Computer-Assisted Intervention. vol. 11769, pp. 257–265 (2019)
13. Hong, X., Tang, F., Wang, L., Chen, J.: Unsupervised deep learning enables real-time image registration of fast-scanning optical-resolution photoacoustic microscopy. Photoacoustics **38**, 100632 (2024)
14. Jiang, H., Karpur, A., Cao, B., Huang, Q., Araujo, A.: OmniGlue: Generalizable Feature Matching with Foundation Model Guidance. In: Proc. of Computer Vision and Pattern Recognition. pp. 19865–19875 (2024)
15. Kikkawa, R., Sekiguchi, H., Tsuge, I., Saito, S., Bise, R.: Semi-Supervised Learning With Structured Knowledge For Body Hair Detection In Photoacoustic Image. In: 2019 IEEE 16th International Symposium on Biomedical Imaging (ISBI 2019). pp. 1411–1415 (2019)
16. Klein, S., Staring, M., Murphy, K., Viergever, M., Pluim, J.: Elastix: A Toolbox for Intensity-Based Medical Image Registration. IEEE Transactions on Medical Imaging **29**(1), 196–205 (2010)
17. Liu, M., Chen, W., Wang, C., Peng, H.: A Multiscale Ray-Shooting Model for Termination Detection of Tree-Like Structures in Biomedical Images. IEEE Transactions on Medical Imaging **38**(8), 1923–1934 (2019)
18. Lowe, D.G.: Distinctive Image Features from Scale-Invariant Keypoints. International Journal of Computer Vision **60**(2), 91–110 (2004)
19. Ma, J., Jiang, X., Fan, A., Jiang, J., Yan, J.: Image matching from handcrafted to deep features: A survey. International Journal of Computer Vision **129**(1), 23–79 (2021)
20. Mok, T.C.W., Chung, A.C.S.: Large Deformation Diffeomorphic Image Registration with Laplacian Pyramid Networks. In: Med. Image Comput. Comput. Assist. Interv. – MICCAI 2020. pp. 211–221 (2020)
21. Mok, T.C.W., Chung, A.C.S.: Affine Medical Image Registration with Coarse-to-Fine Vision Transformer. In: Proc. of Computer Vision and Pattern Recognition. pp. 20803–20812 (2022)
22. Nagae, K., Asao, Y., Sudo, Y., Murayama, N., Tanaka, Y., Ohira, K., Ishida, Y., Otsuka, A., Matsumoto, Y., Saito, S., Furu, M., Murata, K., Sekiguchi, H., Kataoka, M., Yoshikawa, A., Ishii, T., Togashi, K., Shiina, T., Kabashima, K., Toi, M., Yagi, T.: Real-time 3D Photoacoustic Visualization System with a Wide Field of View for Imaging Human Limbs. F1000Res **7**, 1813 (2019)
23. Oliveira, F.P., Tavares, J.M.R.: Medical image registration: A review. Computer Methods in Biomechanics and Biomedical Engineering **17**(2), 73–93 (2014)
24. Rister, B., Horowitz, M.A., Rubin, D.L.: Volumetric Image Registration From Invariant Keypoints. IEEE Transactions on Image Processing **26**(10), 4900–4910 (2017)
25. Rublee, E., Rabaud, V., Konolige, K., Bradski, G.: ORB: An efficient alternative to SIFT or SURF. In: 2011 International Conference on Computer Vision. pp. 2564–2571 (2011)

26. Shen, L., Liu, M., Wang, C., Guo, C., Meijering, E., Wang, Y.: Efficient 3D Junction Detection in Biomedical Images Based on a Circular Sampling Model and Reverse Mapping. IEEE Journal of Biomedical and Health Informatics **25**(5), 1612–1623 (2021)
27. Thirion, J.P.: Image matching as a diffusion process: An analogy with Maxwell's demons. Medical Image Analysis **2**(3), 243–260 (1998)
28. Tustison, N.J., Cook, P.A., Holbrook, A.J., Johnson, H.J., Muschelli, J., Devenyi, G.A., Duda, J.T., Das, S.R., Cullen, N.C., Gillen, D.L., Yassa, M.A., Stone, J.R., Gee, J.C., Avants, B.B.: The ANTsX ecosystem for quantitative biological and medical imaging. Scientific Reports **11**(1), 9068 (2021)
29. Yu, E.M., Wang, A.Q., Dalca, A.V., Sabuncu, M.R.: KeyMorph: Robust Multimodal Affine Registration via Unsupervised Keypoint Detection. In: Proceedings of The 5th International Conference on Medical Imaging with Deep Learning. pp. 1482–1503 (2022)
30. Yu, Q., Liao, Y., Liu, K., He, Z., Zhao, Y., Li, F., Shan, T.: Registration of photoacoustic tomography vascular images: Comparison and analysis of automatic registration approaches. Front. Phys. **10**, 1045192 (2022)
31. Zhou, Z., Liu, X., Long, B., Peng, H.: TReMAP: Automatic 3D Neuron Reconstruction Based on Tracing, Reverse Mapping and Assembling of 2D Projections. Neuroinform **14**(1), 41–50 (2016)